ESKİŞEHİR TECHNICAL UNIVERSITY JOURNAL OF SCIENCE AND TECHNOLOGY
A- APPLIED SCIENCES AND ENGINEERING

2021, 22(1), pp. 99- 117, DOI: 10.18038/estubtda.766590

VIBRATION CHARACTERISTICS OF NONUNIFORM BLADES MADE OF FUNCTIONALLY GRADED MATERIAL

Burak KILIÇ [1], Selim ŞAHİN [2], Özge ÖZDEMİR [3] *

[1] Aeronautical Engineering Department, Faculty of Aeronautics and Astronautics, İstanbul Technical University, İstanbul, Turkey
[2] Aeronautical Engineering Department, Faculty of Aeronautics and Astronautics, İstanbul Technical University, İstanbul, Turkey
[3] Aeronautical Engineering Department, Faculty of Aeronautics and Astronautics, İstanbul Technical University, İstanbul, Turkey

ABSTRACT

The purpose of this study is to examine the vibration characteristics of a rotating blade whose material distribution varies in the spanwise direction. Formulations for functionally graded materials and beam structural models are carried out in detail and the results are displayed in several figures and tables which is a significant source of information for the authors working in this area. Different parameters such as angular speed, radius of the hub, material properties, power law index parameter, boundary conditions and slenderness ratio are considered in the formulation. Finite Element Method where the element matrices are obtained from potential and kinetic energy expressions is applied as the solution procedure. Results of the study are validated with open literature in several tables and figures.

Keywords: Functionally Graded, Helicopter Blade, Finite Element Analysis, Structural Vibration

1. INTRODUCTION

Helicopters are subjected to vibration for various reasons during the flight. Determination of the frequency values and the normal modes is required to perform the vibration analysis in the rotor blade design process correctly. Many numerical and approximate calculation methods are used in the vibration and natural frequency calculations and the Finite Element Analysis (FEA) is among the most efficient methods.

Air and space vehicles, wind turbines, helicopter blades, turbine rotors, defence and civil industries, ship and automotive sectors are among the engineering areas where composite materials have been mostly preferred due to their advantages, i.e. light weight and high strength/stiffness-to-weight ratios. However, composite materials have some limitations. For instance, stress concentration near interlayer surfaces is high because of the sudden changes in mechanical properties and this limitation may cause severe material failures. Moreover, the adhesive layer may get cracked when the temperature is low and it may creep at high temperature. Functionally graded materials, FGMs, are considered to be the new generation composite materials. The variation character of their material properties is continuous through the structure so stress concentrations do not occur. Survivability in high temperatures by maintaining structural integrity is among the outstanding properties of FGMs. Although many different material combinations have been studied for FGMs, the most widely used one is the ceramic-metal combination where the ceramic reduces heat transfer to protect metal from corrosion and oxidation, whereas metal provides strength, higher fracture toughness, etc.

Structural components used in engineering are mostly beams and beam structures. Different material types, i.e. homogeneous, composite, functionally graded, etc. are used in these structural components to

*Corresponding Author: ozdemirozg@itu.edu.tr
Received: 08.07.2020 Published: 26.03.2021

meet different engineering design requirements. Both in conventional structural applications and in advanced structural applications, including electric-thermal-structural systems, FGMs are commonly used as harvesters, sensors and actuators. Therefore, many researchers have been studying these materials for different application areas. Due to the increasing application trend of FGMs, their vibration properties have been examined by applying different beam theories.

The concept of FGMs was originated from a team of material scientists working on thermal barrier materials [1] and nowadays, production areas and application fields are increasing day by day with the development of additive manufacturing technology and powder metallurgy of the material properties. Sankar [2] studied FGM beams with simply-simply supported end conditions under the effect of transverse loading where the beam elasticity modulus changes through the beam thickness. Aydogdu and Taskin [3] studied FGM beams with simply supported end conditions where Modulus of Elasticity changes with respect to a power and an exponential rule in the transverse direction. Chakraborty et al. [4] developed a new beam element to study the thermoelastic behavior of functionally graded beam structures. Goupee and Senthil [5] optimized the natural frequencies of FGM beams by changing the material distribution via a genetic algorithm methodology. Xiang and Yang [6] analysed a thermally presetressed nonuniform FGM beam in the free and forced vibration cases. Piovan and Sampoia [7] employed formulas considering shear-deformation and nonlinear relationship between strain and displacement to study the dynamic behavior of rotating FGM beams. Both the free vibration and the harmonically forced vibration of FGM Euler-Bernoulli beams are studied by Simsek and Kocaturk [8]. Free vibration of curved beams made of FGM in the out of plane direction is analysed by Malekzadeh et al. [9] where temperature dependent material properties are considered. Huang and Li [10] studied free vibration of nonuniform axially functionally graded beams with variable flexural rigidity and mass density. Free vibration and stability analyses of Timoshenko beams with nonuniform cross-sections was studied by Shahba et al [11] by employing an energy based finite element solution. Additionally, several review papers have been published in recent years about the modelling, buckling, stability and vibration characteristics of FGM structures [12, 13].

In this study, FG blades whose material distribution changes in the spanwise direction are modeled and vibration analyses are performed. In these studies, beam models with fixed-free and fixed-fixed boundary conditions and different material distribution properties are investigated. For developing the mathematical models and for the solution, finite element method (FEM) is used. The blade formulations are derived for both Euler-Bernoulli and Timoshenko beam theories to inspect the effect of different parameters on the vibration characteristics. For each beam theory, both the stiffness matrix and the mass matrix are derived from the energy expressions. In the solution part, effects of different parameters such as hub rotating speed, material properties, power law index parameter, different boundary conditions, rotary inertia and shear deformation are investigated. Results of the study are validated with open literature in several tables and figures.

2. MATERIAL and METHOD

2.1. Functionally Graded Nonuniform Blade Model

In this study, vibration analysis is carried out for an Axially Functionally Graded nonuniform blade model which is shown in Figure 1.

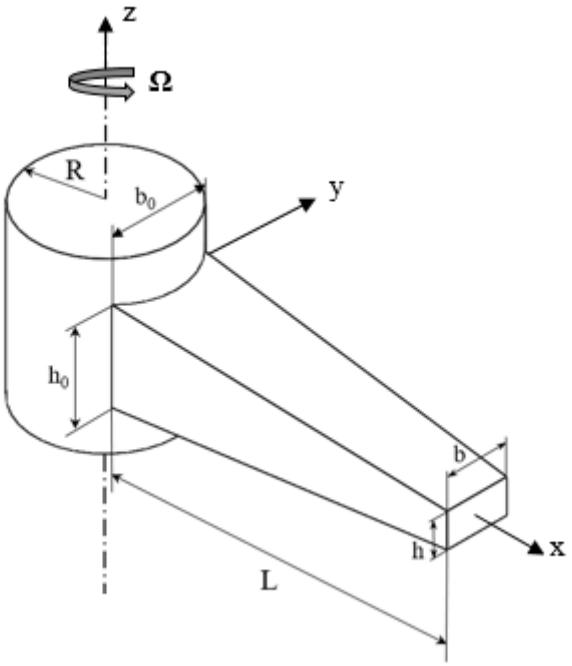

Figure 1. Rotating, axially functionally graded nonuniform beam model

Here a blade having a constant rotational velocity, Ω, is fixed to a rigid hub of radius R at point O. The origin of the right-handed Cartesian coordinate system is located at the root of the blade and the x-axis is directed along the blade while the rotational axis and the z-axis are parallel.

The blade is modeled as a beam structure with variable cross sectional dimensions and material properties along the x-axis. The beam model has two different material properties, i.e. ceramic and metal, in different compositions from the fixed to the free end. Additionally, the beam tapers linearly from a height of h_0 at the root to h at the free end in the xz plane and from a breadth b_0 to b in the xy plane.

Beam material properties vary continuously in the longitudinal direction, i.e. x-axis, via a simple power law. The rule of mixture states that $T(x)$, i.e. the effective material property such as the Elasticity modulus and material density. The other properties can be expressed as given by Equations (1a)-(1e) where α is the power law index parameter that is a positive number and that defines the material variation characteristic along the x-axis.

$$T(x)=(T_R-T_L)\left(\frac{x}{L}\right)^{\alpha}+T_L \quad , \quad \alpha \geq 0 \tag{1a}$$

$$E(x) = (E_R - E_L)\left(\frac{x}{L}\right)^{\alpha} + E_L \tag{1b}$$

$$G(x) = (G_R - G_L)\left(\frac{x}{L}\right)^{\alpha} + G_L \tag{1c}$$

$$\nu(x) = (\nu_R - \nu_L)\left(\frac{x}{L}\right)^{\alpha} + \nu_L \tag{1d}$$

$$\rho(x) = (\rho_R - \rho_L)\left(\frac{x}{L}\right)^{\alpha} + \rho_L \tag{1e}$$

where $(\ )_R$ and $(\ )_L$ are the material properties , i.e. elasticity modulus E, shear modulus G, Poisson's ratio, v and material density, ρ at the right hand side and left hand side of the beam, respectively as given in Figure 2.

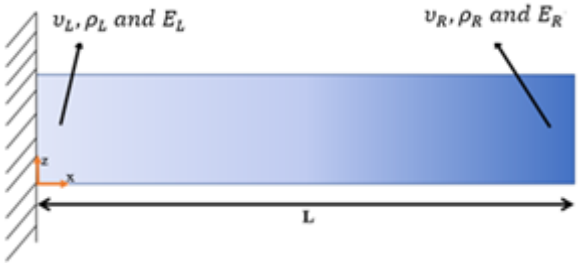

Figure 2. Material variation in an axially functionally graded beam model

The expressions for the geometrical dimensions and the cross-sectional preoperties of a beam that is double tapered are

$$b(x) = b_0\left(1 - c_b\frac{x}{L}\right)^m \tag{2a}$$

$$h(x) = h_0\left(1 - c_h\frac{x}{L}\right)^n \tag{2b}$$

$$A(x) = A_0\left(1 - c_h\frac{x}{L}\right)^n\left(1 - c_b\frac{x}{L}\right)^m \ where\ \ A_0 = b_0h_0 \tag{2c}$$

$$I_y(x) = I_{y0}\left(1 - c_h\frac{x}{L}\right)^{3n}\left(1 - c_b\frac{x}{L}\right)^m \ where\ \ I_{y0} = \frac{1}{12}b_0h_0^3 \tag{2d}$$

Equation (3a) expresses the breadth taper ratio, c_b while Equation (3b) expresses the height taper ratio, c_h . The beam formulation is achieved in a way to let the beam get different taper ratio values in different planes so c_b and c_h do not have to be the same.

$$c_h = 1 - \frac{h_0}{h} \tag{3a}$$

$$c_b = 1 - \frac{b_0}{b} \tag{3b}$$

The exponents n and m get values depending on the taper type of the beam. In this study, a beam structure that tapers in two planes in a linear manner is considered so n = 1 and m = 1 for this study.

2.2. Energy Expressions

In this section, energy expressions are given both for rotating, nonuniform AFG Euler-Bernoulli and Timoshenko beam models. Details of the derivation can be found in Ref. [14-16] in great detail by using several explanatory figures and tables.

The potential energy expressions are given for Euler-Bernoulli and Timoshenko beam models in Equation (4a) and Equation (4b), respectively.

$$U_{Euler} = \frac{1}{2}\left[E(x)I_y(x)(\theta')^2 + F_{CF}(x)(w')^2\right]dx + C_1 \tag{4a}$$

$$U_{Timoshenko} = \frac{1}{2}\int_0^{L_e}\left[E(x)I_y(x)(\theta')^2 + kA(x)G(x)(w'-\theta)^2 + F_{CF}(x)(w')^2\right]dx + C_2 \tag{4b}$$

where the centrifugal force is

$$F_{CF}(x) = \int_x^L \rho A\Omega^2(R+x)dx \tag{5}$$

In Equation (4b), the first term is the strain energy due to transverse displacement while the second term is the strain energy due to shear which is a result of the Timoshenko beam formulation.

The kinetic energy expressions are given for Euler-Bernoulli and Timoshenko beam models in Equation (6a) and Equation (6b), respectively.

$$T_{Euler} = \frac{1}{2}\int_0^L (\rho A\dot{w}^2 + \rho I_y(\dot{w}')^2 + \rho I_y\Omega^2(w')^2)dx + D_1 \tag{6a}$$

$$T_{Timoshenko} = \frac{1}{2}\int_0^{L_e}\left(\rho A\dot{w}^2 + \rho I_y\dot{\theta}^2 + \rho I_y\Omega^2\theta^2\right)dx + D_2 \tag{6b}$$

In the Equations (4a)-(6b), C_1, C_2, D_1 and D_2 are the integration constants.

2.3. Finite Element Modeling

Finite element representation of the functionally graded and nonuniform rotating beam model is shown in Figure 3.

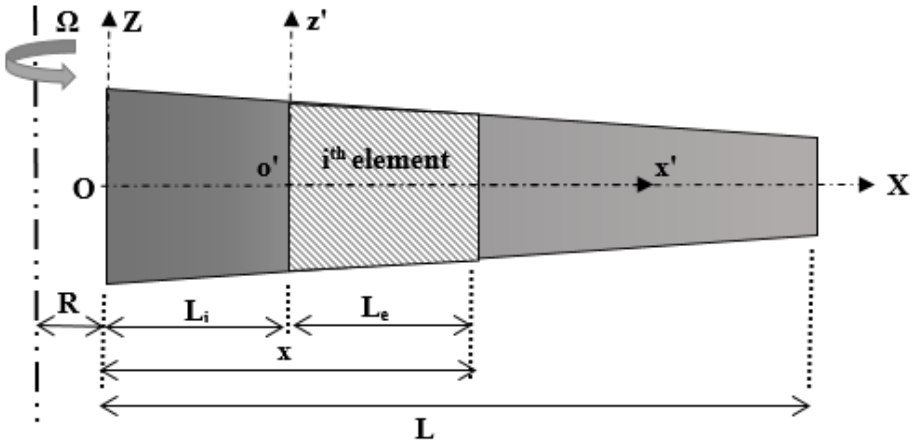

Figure 3. FE model of a FG nonuniform rotating beam

where L_i is the offset of each element from the rotational axis and L_e is the element length. Depending on the analysis, L_e may get different values for each element but in this study, the beam model is divided into elements of the same length. Here XYZ and $x'y'z'$ are the global and local coordinates, respectively.

When a beam that rotates about a fixed axis is studied, new terms are added to the element stiffness matrices resulting from the centrifugal force. Considering the finite element model, given in Figure 3, the centrifugal force, i.e. Equation (5), can be expressed as follows where N_e is the number of elements used in the FE formulation.

$$F_{CF}(x) = \rho A\Omega^2[R(L - L_i - x') + \frac{1}{2}(L - L_i - x')(L - L_i + x')] \tag{7a}$$

$$L_i = (i-1)\frac{L}{N_e}, \qquad i = 1, 2, \ldots., N_e \tag{7b}$$

Euler Bernoulli beam finite element modeling

In Figure 4, an Euler Bernoulli beam finite element model which has four degrees of freedom is shown. Due to the Euler beam theory, shear effects are not considered and the degree of freedom is two, i.e. transverse displacement, *w* and rotation θ at each node. The rotation angle is defined as the slope at each node, so $\theta = w'$.

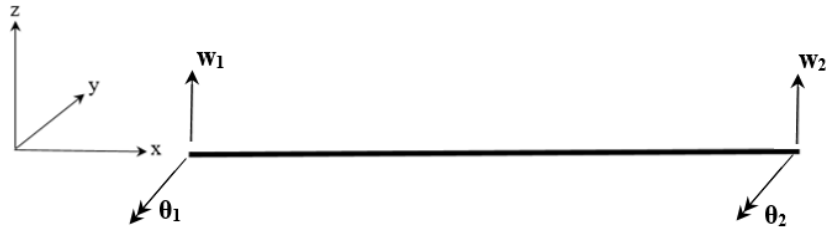

Figure 4: FE model of an Euler Bernoulli beam

Polynomials are defined to express the displacement field of the Euler-Bernoulli beam [17]

$$w = a_0 + a_1 x + a_2 x^2 + a_3 x^3 \tag{8a}$$

$$\theta = w' = a_1 + 2a_2 x + 3a_3 x^2 \tag{8b}$$

Considering the displacement field polynomials given by Equation (8a) and Equation (8b), the nodal displacements are defined at the 1st node and at the 2nd node, respectively as follows

$$\begin{Bmatrix} w_1 \\ \theta_1 \\ w_2 \\ \theta_2 \end{Bmatrix} = \begin{bmatrix} 1 & 0 & 0 & 0 \\ 0 & 1 & 0 & 0 \\ 1 & L_e & L_e^2 & L_e^3 \\ 0 & 1 & 2L_e & 3L_e^2 \end{bmatrix} \begin{Bmatrix} a_0 \\ a_1 \\ a_2 \\ a_3 \end{Bmatrix} \tag{9}$$

Here, $(\ \ )_1$ are the displacement values of the 1st node while $(\ \ )_2$ are the displacements on the 2nd node.

The displacement field vector, $\{q\}$ and the nodal displacement vector, $\{q_e\}$ are related to each other by the matrix of shape functions, [N].

$$\{q\} = [N]\{q_e\} \tag{10}$$

where

$$\{q\} = \{w \quad \theta\}^T \tag{11a}$$

$$\{q_e\} = \{w_1 \quad \theta_1 \quad w_2 \quad \theta_2\}^T \tag{11b}$$

$$[N] = [N_w \quad N_\theta]^T \tag{11c}$$

Here the expressions of the shape functions are

$$[N_w] = \left\{1 - \frac{3x^2}{L^2} - \frac{2x^3}{L^3} \quad x - \frac{2x^2}{L} + \frac{x^3}{L^2} \quad \frac{3x^2}{L^2} - \frac{2x^3}{L^3} \quad -\frac{x^2}{L} + \frac{x^3}{L^2}\right\} \tag{12a}$$

$$[N_\theta] = \left\{-\frac{6x}{L^2} + \frac{6x^2}{L^3} \quad 1 - \frac{4x}{L} + \frac{3x^2}{L^2} \quad \frac{6x}{L^2} - \frac{6x^2}{L^3} \quad -\frac{2x}{L} + \frac{3x^2}{L^2}\right\} \tag{12b}$$

Here, $[N_w]$ and $[N_\theta]$ are the normal modes associated with the transverse motion *w* and the rotation angle, θ, respectively and $[\ \ ]^T$ is the transpose of a matrix.

Considering the effect of the centrifugal force and substituting the shape functions, i.e. Equation (12a) and Equation (12b), into the energy expressions the element stiffness and mass matrices, i.e. $[K^e]$ and $[M^e]$, are obtained as follows

$$[K^e] = \frac{1}{2}\int_0^{L_e} \left(E(x)I_y(x)\left[\frac{dN_\theta}{dx}\right]^T \left[\frac{dN_\theta}{dx}\right] + F_{MK}(x)\left[\frac{dN_w}{dx}\right]^T \left[\frac{dN_w}{dx}\right]\right) dx \tag{13a}$$

$$[M^e] = \frac{1}{2}\int_0^{L_e} \left(\rho(x)A(x)[N_w]^T[N_w] + \rho(x)I_y(x)[N_\theta]^T[N_\theta]\right) dx \tag{13b}$$

Timoshenko beam finite element modeling

In Figure 5, a Timoshenko beam finite element model which has six degrees of freedom is shown. Due to the Timoshenko beam theory, shear effects are considered and the degree of freedom is three, i.e. transverse displacement, *w*, rotation angle θ and shear angle, φ at each node.

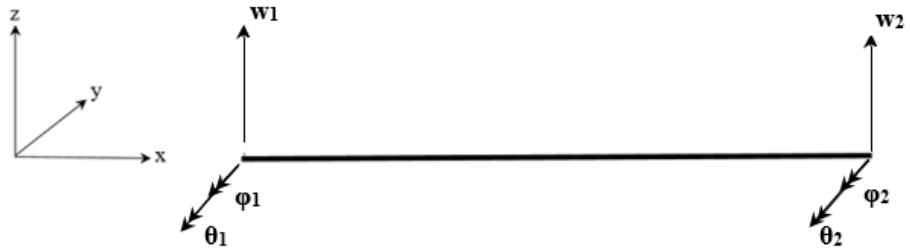

Figure 5: FE model of a Timoshenko beam

Polynomials are defined to express the displacement field of the Timoshenko beam [17]

$$w = a_0 + a_1 x + a_2 x^2 + a_3 x^3 \tag{14a}$$

$$\varphi = a_4 + a_5 x \tag{14b}$$

$$\theta = w' - \varphi = a_1 - a_4 + (2a_2 - a_5)x + 3a_3 x^2 \tag{14c}$$

Considering the displacement field polynomials given by Equations (14a)-(14c), the nodal displacements are defined at the 1st node and at the 2nd node, respectively as follows.

$$\begin{Bmatrix} w_1 \\ \theta_1 \\ \varphi_1 \\ w_2 \\ \theta_2 \\ \varphi_2 \end{Bmatrix} = \begin{bmatrix} 1 & 0 & 0 & 0 & 0 & 0 \\ 0 & 1 & 0 & 0 & -1 & 0 \\ 0 & 0 & 0 & 0 & 1 & 0 \\ 1 & L_e & L_e^2 & L_e^3 & 0 & 0 \\ 0 & 1 & 2L_e & 3L_e^2 & -1 & -L_e \\ 0 & 0 & 0 & 0 & 1 & L_e \end{bmatrix} \begin{Bmatrix} a_0 \\ a_1 \\ a_2 \\ a_3 \\ a_4 \\ a_5 \end{Bmatrix} \tag{15}$$

From Equation (10),

$$\{q\} = \{w \quad \theta \quad \varphi\}^T \tag{16a}$$

$$\{q_e\} = \{w_1 \quad \theta_1 \quad \varphi_1 \quad w_2 \quad \theta_2 \quad \varphi_2\}^T \tag{16b}$$

$$[N] = [N_w \quad N_\theta \quad N_\varphi]^T \tag{16c}$$

Here $[N_w]$, $[N_\theta]$ and $[N_\varphi]$ are the shape functions associated with the transverse displacement, *w*, rotation angle due to transverse displacement, θ and shear angle, φ, respectively.

$$[N_w] = \left\{1 - \frac{3x^2}{{L_e}^2} + \frac{2x^3}{{L_e}^3} \quad x - \frac{2x^2}{L_e} + \frac{x^3}{{L_e}^2} \quad x - \frac{2x^2}{L_e} + \frac{x^3}{{L_e}^2} \quad \frac{3x^2}{{L_e}^2} - \frac{2x^3}{{L_e}^3} \quad -\frac{x^2}{L_e} + \frac{x^3}{{L_e}^2} \quad -\frac{x^2}{L_e} + \frac{x^3}{{L_e}^2}\right\} \tag{17a}$$

$$[N_\theta] = \left\{-\frac{6x}{{L_e}^2} + \frac{6x^2}{{L_e}^3} \quad 1 - \frac{4x}{L_e} + \frac{3x^2}{{L_e}^2} \quad -\frac{3x}{L_e} + \frac{3x^2}{{L_e}^2} \quad \frac{6x}{{L_e}^2} - \frac{6x^2}{{L_e}^3} \quad -\frac{2x}{L_e} + \frac{3x^2}{{L_e}^2} \quad -\frac{3x}{L_e} + \frac{3x^2}{{L_e}^2}\right\} \tag{17b}$$

$$[N_\varphi] = \left\{0 \quad 0 \quad 1 - \frac{x}{L_e} \quad 0 \quad 0 \quad \frac{x}{L_e}\right\} \tag{17c}$$

Considering the effect of the centrifugal force and substituting the shape functions into the potential and kinetic energy expressions, the element stiffness matrix, $[K^e]$, and element mass matrix, $[M^e]$, are obtained as follows

$$[K^e] = \frac{1}{2}\int_0^L \left(E(x)I_y(x)\left[\frac{dN_\theta}{dx}\right]^T\left[\frac{dN_\theta}{dx}\right] + kA(x)G(x)\left(\left[\frac{dN_w}{dx}\right] - N_\theta\right)^T\left(\left[\frac{dN_w}{dx}\right] - N_\theta\right) + F_{CF}(x)\left[\frac{dN_w}{dx}\right]^T\left[\frac{dN_w}{dx}\right]\right) dx \tag{18a}$$

$$[M^e] = \frac{1}{2}\int_0^L \left(\rho(x)A(x)[N_w]^T[N_w] + \rho(x)I_y(x)[N_\theta]^T[N_\theta]\right) dx \tag{18b}$$

Reduced global matrices and modal analysis

Depending on the element number used in the FE modeling, all the element matrices are assembled by considering the finite element rules to get the global matrices. The BC's are applied to the global matrices to get the reduced matrix system of equations

$$[M]\{\ddot{q}\} + [K]\{q\} = \{0\} \tag{19}$$

where $[M]$ and $[K]$ are the reduced global mass and reduced global stiffness matrices, respectively.

Modal analysis is applied to Equation (19) to calculate the natural frequencies, ω as follows.

$$\det\left[[K] - \omega^2[M]\right] = 0 \tag{20}$$

3. THE RESEARCH FINDINGS AND DISCUSSION

In this section, flapwise bending vibration analysis of both Euler-Bernoulli and Timoshenko beams that taper in both planes and that have material variation in the axial direction are carried out. Several parameters, i.e. taper ratios for nonuniformity, power law index parameter for material distribution, slenderness ratio, rotational speed, hub radius parameter, etc. are considered for the vibration analysis.

The normalized parameters used in the tables and graphics are given by

$$\bar{\omega} = \omega \sqrt{\rho A_0 L^4 / E I_{y0}} \tag{21a}$$

$$r = \sqrt{I_{y0} / A_0 L^2} \tag{21b}$$

$$\sigma = R / L \tag{21c}$$

where the properties given in the paranthesis $(...)_0$ are the ones defined at the root of the blade where x=0. Here, $\bar{\omega}$ is the normalized natural frequency, r is the slenderness ratio and σ is the normalized hub radius.

Several tables and figures which are expected to be a good source for the researchers who study in this field to analyse the initial models for helicopter blades are presented in this study. When the results are compared with the ones in open literature, it is noticed that there is a very good agreement between the results which proves the correctness and accuracy of the studies in this paper.

3.1. Homogeneous Nonuniform Beams

In this section, vibration characteristics are examined for both Euler Bernoulli and Timoshenko beams that have taper effects and homogeneous material properties.

Euler-Bernoulli beam results

In this case, vibration characterics of a rotating/nonrotating, tapered Euler-Bernoulli beam having clamped free boundary conditions is examined. The geometrical and material properties of the beam model are given in Table 1.

Table 1. Geometrical and material properties of the homogeneous tapered Euler Bernoulli beam

Beam Height, $\mathbf{h_0 = 0.01\ m}$	Material Density, $\boldsymbol{\rho = 7850\ kg/m^3}$
Beam Breadth , $\mathbf{b_0 = 0.1\ m}$	Elasticity Modulus, $\mathbf{E = 206.8\ GPa}$
Beam Length, $\mathbf{L = 2\ m}$	Poisson's Ratio, $\boldsymbol{\upsilon = 0.3}$
Hub radius, R=0 m (Clamped beam)	

Variation of the normalized natural frequencies with respect to taper ratios, c_h and c_b is introduced in Table 2 and Table 3 for homogeneous Euler-Bernoulli beams model with fixed-free end conditions. The calculated results are compared with the ones in open literature and a very good agreement between the results is observed.

Table 2. Effects of taper ratios on the natural frequencies of a nonrotating Euler-Bernoulli beam

	c_h							
	0		**0.3**		**0.6**		**0.8**	
c_b	**Present**	**Ref.[18]**	**Present**	**Ref.[18]**	**Present**	**Ref.[18]**	**Present**	**Ref.[18])**
0	3.5160	3.5160	3.6656	3.6667	3.9258	3.9343	4.2631	4.2925
	22.0338	22.0345	19.8903	19.8806	17.5318	17.4879	15.8180	15.7427
	61.6924	61.6972	53.3599	53.3222	44.2046	44.0248	37.2405	36.8846
	120.8850	120.9020	103.3440	103.2670	83.9397	83.5541	68.9108	68.1164
0.3	3.9135	3.9160	4.0632	4.0669	4.3250	4.3362	4.6665	4.6991
	22.7801	22.7860	20.5609	20.5555	18.1217	18.0803	16.3487	16.2744
	62.4253	62.4361	54.0474	54.0152	44.8340	44.6583	37.8171	37.4635
	121.6240	121.6480	104.0450	103.9750	84.5900	84.2101	69.5110	68.7209
0.6	4.5670	4.5853	4.7175	4.7372	4.9929	5.0090	5.3471	5.3761
	23.9833	24.0211	21.6466	21.6699	19.1775	19.0649	17.2032	17.1657
	63.6990	63.7515	55.2170	55.2224	45.8302	45.7384	38.6497	38.4392
	122.9480	123.0250	105.2630	105.2410	85.5567	85.3438	70.2244	69.7438
0.8	5.3625	5.3976	5.5170	5.5529	5.7882	5.8288	6.1431	6.1964
	25.5754	25.6558	23.0914	23.1578	20.3607	20.3952	18.3800	18.3855
	65.6300	65.7470	56.9379	57.0157	47.3322	47.3051	39.9876	39.8336
	125.1050	125.2640	107.1490	107.2310	87.1879	87.0561	71.6519	71.2418

In Table 2, it is noticed that increasing taper ratios have increasing effects on the natural frequencies and the effect of the breadth taper ratio, c_b, is more dominant.

Variation of the normalized natural frequencies with respect to the taper ratios and the rotational speed parameter is given in Table 3.

Table 3. Effects of taper ratios and rotational speed on the natural frequencies of a rotating Euler-Bernoulli beam

	Ω							
	2		**4**		**6**		**8**	
	Present	**Ref.[19]**	**Present**	**Ref.[19]**	**Present**	**Ref.[19]**	**Present**	**Ref.[19]**
c_b=0 c_h=0.5	4.527	4.4368	6.1826	5.8788	8.1936	7.6551	10.3337	9.5539
	19.109	18.9366	21.1283	20.6851	24.1151	23.3093	27.7481	26.5437
	48.3031	47.8717	50.4098	49.6456	53.7245	52.4632	58.0238	56.1595
	91.9318	91.0625	94.1133	92.873	97.6306	95.809	102.332	99.7638
c_b=0.5 c_h=0.5	5.3099	5.1564	7.054	6.4726	9.2283	8.1663	11.5754	10.0192
	20.2771	20.0733	22.283	21.5749	25.2655	23.8684	28.9117	26.7454
	49.5292	49.0906	51.6321	50.5938	54.9446	53.0018	59.2468	56.1941
	93.1673	92.3243	95.345	93.8415	98.8577	96.3142	103.555	99.6673

Here Table 3 reveals that as the rotational speed Ω, increases, the natural frequencies increase because the centrifugal force, i.e. Equation (5), which is proportional to the square of the rotational speed makes the beam stiffer.

Timoshenko beam results

Table 4 gives the material and geometrical properties of the homogeneous nonuniform Timoshenko beam model. In Table 5, variation of the Timoshenko beam natural frequencies with respect to the taper ratio parameters are tabulated. The case, given in Table 5, demonstrates a beam that has the same taper in both planes; i.e. c_h=c_b. and that has fixed-free boundary conditions.

Table 4. Geometrical and material properties of homogeneous Timoshenko beam

Beam Height, $h = 0.037$ m	Material Density, $\rho = 7860$ kg/ m^3
Beam Length, $L = 0.24$ m	Elasticity Modulus, $E = 210$ GPa
Slenderness Ratio, r=0.01	Poisson's Ratio, $\upsilon = 0.3$
Shear Correction Factor, k = 5/6	

Table 5. Effects of taper ratios on the natural frequencies of a Timoshenko beam (fixed-free)

ch	Experimental Study Ref.[20]	Mathematical Modelling Ref.[20]	Present
0.1	3.4821	3.4956	3.4976
	18.941	19.1962	19.2561
	46.8812	47.5057	47.8338
	80.8891	82.0774	82.9644
0.3	3.5962	3.6076	3.6068
	17.9951	18.2044	18.2602
	43.861	44.3941	44.6912
	76.1284	77.1983	78.0033
0.5	3.7462	3.7665	3.7606
	16.9821	17.0617	17.1278
	39.9951	40.7118	41.0235
	69.7561	71.1402	71.9314

Variation of the first four natural frequencies of homogeneous Euler-Bernoulli and Timoshenko beams with respect to the height taper ratio, c_h and the breadth taper ratio, c_b are displayed in Figure 6 and Figure 7, respectively. Here, R=0, r=0.08, υ=0.3, k=0.85. The dashed lines show the variation of the Euler-Bernoulli beam natural frequencies while the solid lines show the variation of the Timoshenko beam natural frequencies.

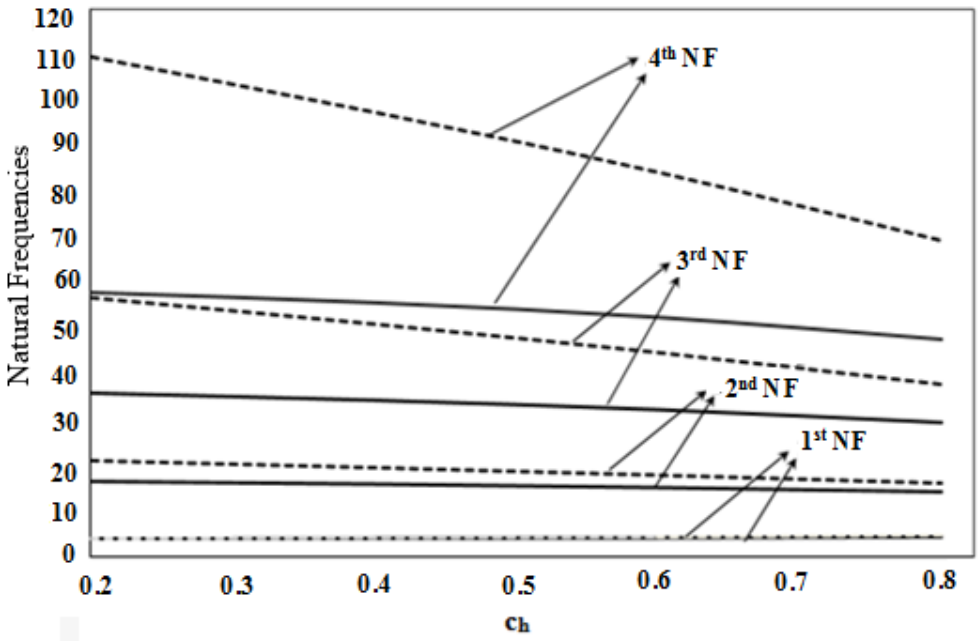

Figure 6. Effect of the height taper ratio, c_h,on the natural frequencies (c_b=0.2)

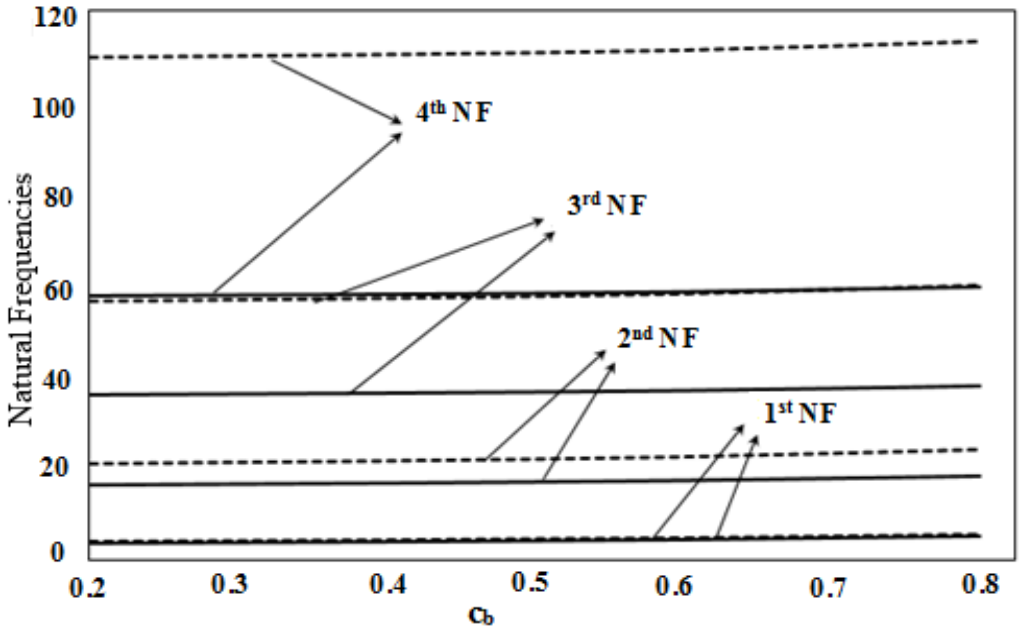

Figure 7. Effect of the breadth taper ratio, c_b,on the natural frequencies (c_h=0.2)

Here Figure 6 and Figure 7 reveal that c_b has less effect on the variation of the natural frequencies while c_h is more dominant. Especially, this difference is more obvious on higher modes. Moreover, Euler-Bernoulli beam frequencies are higher than the Timoshenko beam frequencies due to the decreasing effect of the inverse of the slenderness ratio.

3.2. Axially Functionally Graded Beams

In this section, vibration characteristics are examined for both Euler Bernoulli and Timoshenko beams that have axially functionally graded (AFG) material properties. The beam model used for the analysis is shown in Figure 8 where the beam material is pure ZrO_2 at the fixed end and it is pure Al at the free end.

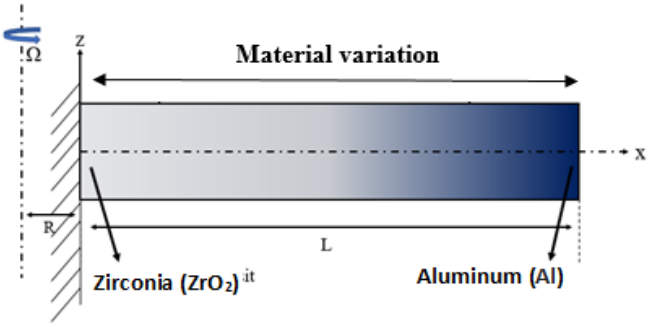

Figure 8. Rotating, axially functionally graded, cantilevered beam

In Table 6, the material properties of Aluminum and Zirconia are displayed.

Table 6. Material properties of the AFG beam

Material Property	Zirconia (ZrO_2)	Aluminum (Al)
Elasticity Modulus, **E**	200 GPa	70 GPa
Material Density, **ρ**	**5700 kg/ m^3**	**2702 kg/ m^3**
Poisson's Ratio, **υ**	0.3	0.3

Euler-Bernoulli beam results

Vibration properties of an AFG Euler-Bernoulli beam is analyzed for hinged-hinged boundary conditions. In Table 7, effect of the taper ratio on the natural frequencies of homogeneous and AFG Timoshenko beam models are tabulated. The results are compared with the ones given by Ref. [21].

Table 7. Natural frequencies of Tapered AFG Euler-Bernoulli beam (hinged-hinged)

cb	Homogeneous Euler Beam				AFG Euler Beam			
	ch				ch			
	0	**0.1**	**0.5**	**0.9**	**0**	**0.1**	**0.5**	**0.9**
0	9.865 9.8696*****	9.361	7.118	3.928	9.569 9.5994*	9.044	6.711	3.425
	39.401	37.409	28.912	18.216	38.265	36.329	28.090	17.833
	88.435	83.980	64.805	40.210	85.985	81.616	62.882	39.028
	156.682	148.833	114.831	70.561	152.736	144.948	111.408	68.141
0.1	9.861	9.354	7.095	3.892	9.550	9.022	6.678	3.386
	39.392	37.405	28.925	18.252	38.268	36.336	28.115	17.882
	88.414	83.966	64.820	40.257	85.986	81.624	62.915	39.089
	156.644	148.804	114.839	70.609	152.726	144.946	111.437	68.203
0.5	9.808	9.281	6.946 6.9566*****	3.676	9.413	8.870	6.470 6.5127*	3.155
	39.389	37.423	29.032	18.494	38.320	36.410	28.285	18.206
	88.388	83.974	64.969	40.582	86.075	81.743	63.162	39.491
	156.563	148.766	114.976	70.959	152.798	145.054	111.695	68.631
0.9	9.525	8.967	6.502	30.974	8.953	8.387	5.904	2.559
	39.397	37.469	29.259	19.115	38.350	36.492	28.614	19.060
	88.539	84.184	65.449	41.553	86.399	82.132	63.845	40.691
	156.810	149.081	115.610	72.137	153.337	145.661	112.605	70.037

*** Ref.[21]**

Effect of the power law index parameter, $\boldsymbol{\alpha}$ on the Modulus of Elasticity, E, of the beam is demonstrated in Figure 9. Here it is noticed that the percentage of Zirconia gets higher with the increasing value of the power law index parameter, α.

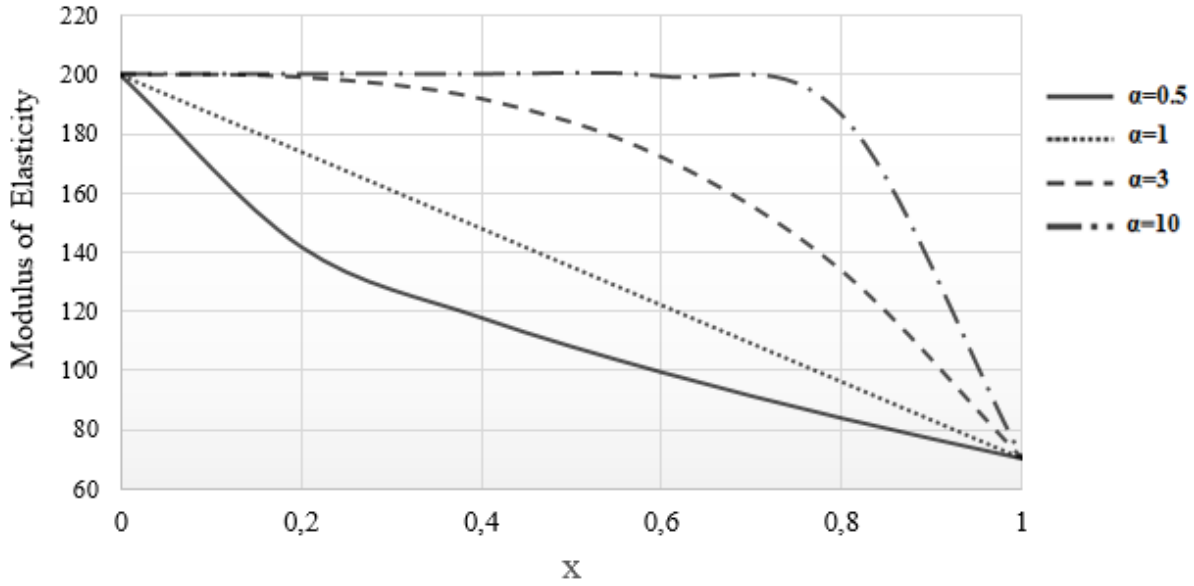

Figure 9. Effect of the power law index parameter, α on the Modulus of Elasticity, E

Timoshenko beam results

Vibration analysis of AFG Timoshenko beam is carried out for the hinged-hinged boundary condition. As an addition to the material properties given in Table 5, $r = 0.01\ m$ is the slenderness ratio, L= $5\ m$ is the beam length and k=5/6 is the shear correction factor.

In Table 8, effect of the power law index parameter, α on the normalized frequencies is tabulated. Here, it is noticed that the natural frequencies increase with the power law index parameter.

Table 8. Natural frequencies of AFG Uniform Timoshenko beam (fixed-free)

Power Law Index Parameter, α	Dimensionless Natural Frequencies			
	Clamped Free		Clamped Clamped	
	Ref.[22]	Present	Ref.[22]	Present
0.3	3.500	3.522	12.870	13.065
	14.250	14.333	26.780	27.052
	30.059	30.059	43.300	43.283
	45.070	45.070	59.000	57.876
0.9	3.900	3.882	12.730	13.107
	15.000	15.114	26.700	27.460
	30.900	31.228	43.490	44.298
	46.000	46.807	59.500	59.599
1.5	3.940	3.959	12.650	12.968
	15.150	15.399	26.650	27.451
	31.580	31.827	43.580	44.653
	47.700	47.826	59.700	60.290
2.1	3.920	3.946	12.600	12.852
	15.250	15.525	26.630	27.390
	31.700	32.215	43.620	44.821
	48.200	48.522	59.740	60.640

In Table 9, variation of the normalized natural frequencies of an AFG Timoshenko beam (α=2) with respect to the taper ratios; i.e. c_h and c_b is given.

Table 9. Natural frequencies of AFG Nonuniform Timoshenko beam (fixed-free)

c_b	c_h						
	Present	**Present**	**Ref.[22]**	**Present**	**Ref.[22]**	**Present**	**Ref.[22]**
	0	**0.1**		**0.3**		**0.5**	
0	3.896	4.008	-	4.282	-	4.654	-
	15.309	15.466	-	15.837	-	16.329	-
	31.727	31.838	-	32.111	-	32.495	-
	47.789	47.896	-	48.172	-	48.587	-
0.1	3.948	4.060	4.049	4.334	-	4.708	-
	15.197	15.349	15.313	33.000	-	16.191	-
	31.323	31.433	31.380	31.703	-	32.081	-
	47.732	47.833	47.823	48.088	-	48.468	-
0.3	4.073	4.186	-	4.461	4.457	4.837	-
	14.887	15.030	-	15.373	15.358	15.832	-
	30.328	30.437	-	30.704	30.680	31.075	-
	46.946	47.037	-	47.266	47.291	47.600	-
0.5	4.244	4.357	-	4.634	-	5.011	5.018
	14.442	14.577	-	14.901	-	15.340	15.349
	29.007	29.117	-	29.382	-	29.751	29.757
	45.351	45.440	-	45.659	-	45.973	46.029

Effects of the rotational speed parameter, $\bar{\Omega}$ and the hub radius parameter, σ on the dimensionless frequencies of a AFG Timoshenko beam that rotates with a constant angular speed is analyzed in Figure 10 and Figure 11 for α=1.

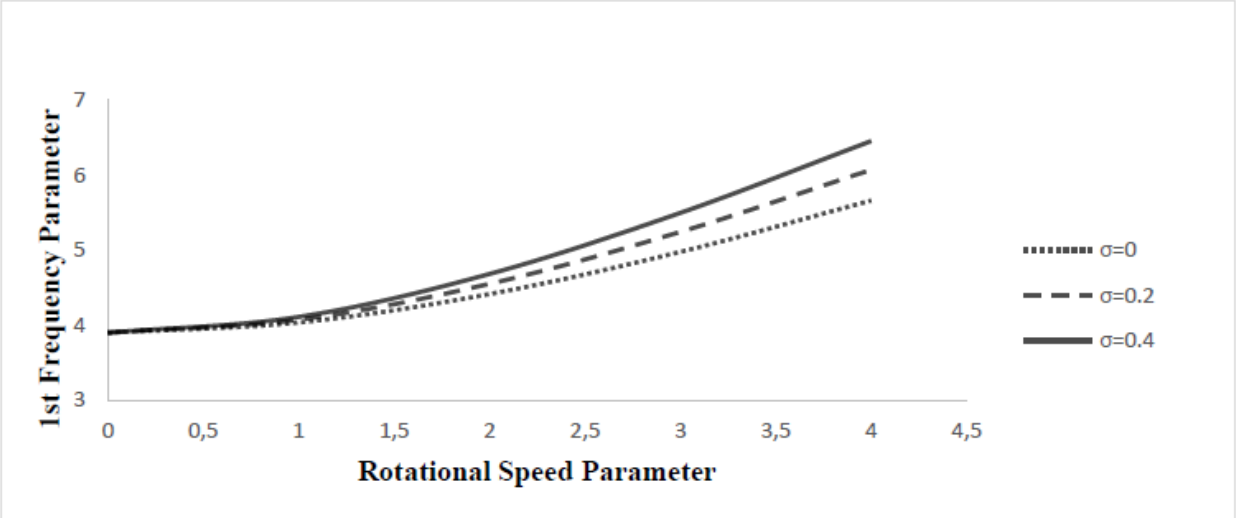

Figure 10. Fundamental frequency variation via hub radius and rotational speed.

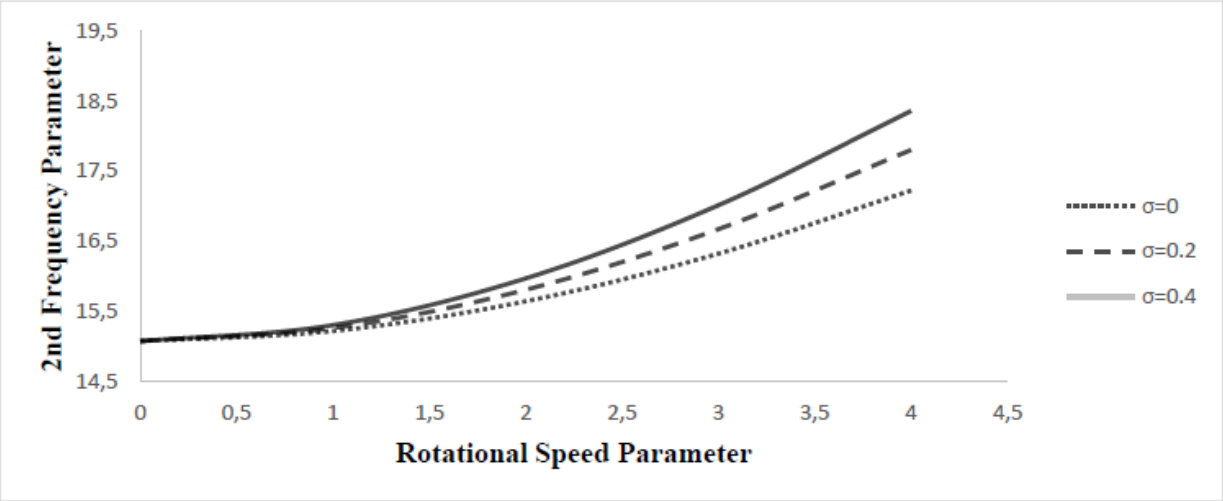

Figure 11. 2nd frequency variation via hub radius and rotational speed.

As it is seen in Figure 10 and Figure 11, the increasing rotational speed increases the natural frequencies and as the hub radius parameter gets larger values, this increasing effect gets more dominant because the centrifugal force becomes more effective on the natural frequencies.

4. CONCLUSION

In this study, finite element formulation of axially functionally graded Euler Bernoulli and Timoshenko beams with different boundary conditions that undergo transverse displacement is derived. The beam models are tapered in one or two planes with different taper ratios. The calculated results are introduced in several figures and tables and compared with the ones in open literature.

Considering the calculated results, the following conclusions are reached:

- The hub rotating speed increases the natural frequencies. This effect becomes more dominant as the hub radius parameter gets larger values.
- Increasing taper ratios have increasing effects on the natural frequencies of Euler Bernoulli and Timoshenko beam models. The increasing effect of the breadth taper ratio, c_b, is more dominant.
- The power law index parameter, i.e. α, increases the natural frequencies and this increasing effect becomes more dominant on higher frequencies.

CONFLICT OF INTEREST

The authors stated that there are no conflicts of interest regarding the publication of this article.

REFERENCES

[1] Loy CT. Lam KY and Reddy JN. Vibration of functionally graded cylindrical shells, Int. J. Mech.Sci. 1999, 41: 309-324.

[2] Sankar BV. An elasticity solution for functionally graded beams, Compos. Sc. Technol. 2001, 61: 689–696.

[3] Aydogdu M, Taskin V. Free vibration analysis of functionally graded beams with simply supported edges, Mater. Des. 2007, 28:1651–1656.

[4] Chakraborty A, Gopalakrishnan S, Reddy JN. A new beam finite element for the analysis of functionally graded materials, J. Mech.Sci. 2003, 45.

[5] Goupee AJ and Senthil SV, Optimization of natural frequencies of bidirectional functionally graded beams, Struct Multidiscip O 2006; 32:473–484.

[6] Xiang HJ and Yang J, Free and forced vibration of a laminated FGM Timoshenko beam of variable thickness under heat conduction, Compos Part B 2008; 39:292–303.

[7] Piovan MT and Sampoia R, A study on the dynamics of rotating beams with functionally graded properties, J Sound Vib 2009; 327:134–143.

[8] Simsek M and Kocaturk T, Free and forced vibration of a functionally graded beam subjected to a concentrated moving harmonic load, Compos Struct 2009; 90: 465–473.

[9] Malekzadeh P, Golbahar MR and Atashi MM, Out-of-plane free vibration of functionally graded circular curved beams in thermal environment, Compos Struct 2010; 92: 541–552.

[10] Huang Y and Li XF, A new approach for free vibration of axially functionally graded beams with non-uniform cross-section, J Sound Vib 2010; 329:2291–2303.

[11] Shahba A, Attarnejad R, Marvi MT and Hajilar S, Free vibration and stability analysis of axially functionally graded tapered Timoshenko beams with classical and non-classical boundary conditions, Compos Part B 2011; 42(4):801-808.

[12] Zahedinejad P, Zhanga C, Zhanga H and Shuaia J, A comprehensive review on vibration analysis of functionally graded beams, Int J Struct Stab Dy 2020; 20 (4), 2030002.

[13] Zhang N, Khan T, Guo H, Shi S, Zhong W and Zhang W, Functionally graded materials: An overview of stability, buckling, and free vibration analysis, Adv Mater Sci Eng 2019; 1354150.

[14] Ozdemir O, Vibration analysis of rotating Timoshenko beams with different material distribution properties, Selçuk University, Int J Sci 2019; 7(2): 272-286.

[15] Kılıç B, Eksenel Fonksiyonel Derecelendirilmiş Rotor Pallerinin Titreşim Analizi, Msc.Thesis, Department of Aeronautical Engineering, Istanbul Technical University, 2019.

[16] Şahin S, İki Eksende Daralan Helikopter Pallerinin Sonlu Elemanlar Metodu ile Titreşim Analizi, Msc.Thesis, Department of Aeronautical Engineering, Istanbul Technical University, 2019.

[17] Hartmann F and Katz C, Structural Analysis with Finite Elements, Springer, 2004.

[18] Downs B, Transverse vibrations of cantilever beams having unequal breadth and depth tapers, J Appl Mech 1977; 44(4): 737-742.

[19] Banerjee JR and Williams FW, Exact Bernoulli–Euler dynamic stiffness matrix for a range of tapered beams, Int J Numer Meth Eng 1985; 21: 2289–2302.

[20] Talebi S and Ariaei A, Vibration analysis of a rotating Timoshenko beam with internal and external flexible connections, Arch Appl Mech 2015; 85(5): 555-572.

[21] Soltani M and Asgarian B, New hybrid approach for free vibration and stability analyses of axially functionally graded Euler-Bernoulli beams with variable cross-section resting on uniform Winkler-Pasternak foundation, Lat Am J Solids Stru 2019; 16(3), e173.

[22] Shahba A, Attarnejad R, Marvi MT and Hajilar S, Free vibration and stability analysis of axially functionally graded tapered Timoshenko beams with classical and non-classical boundary conditions, Compos Part B-Eng 2011; 42(4): 801-808.